# Lateral terrestrial water fluxes in the LSM of WRF Hydro: benefits of a 2D groundwater representation

**Thomas Rummler, Andreas Wagner, Joël Arnault, Harald Kunstmann**

WILEY

# Lateral terrestrial water fluxes in the LSM of WRF-Hydro: Benefits of a 2D groundwater representation

Thomas Rummler[1] 🟢    |    Andreas Wagner[1]    |    Joël Arnault[2] 🟢    |    Harald Kunstmann[1,2]

[1]University of Augsburg, Institute of Geography, Germany

[2]Karlsruhe Institute of Technology, Campus Alpin, Institute of Meteorology and Climate Research, Garmisch-Partenkirchen, Germany

**Correspondence**
Thomas Rummler, University of Augsburg, Institute of Geography, Germany.
Email: thomas.rummler@geo.uni-augsburg.de

**Funding information**
Bavarian State Ministry of Science and the Arts, Grant/Award Number: Bavarian Climate Research Network - Landklif; Deutsche Forschungsgemeinschaft, Grant/Award Numbers: AR 1183/2-1, KU 2090/10-1; Research Foundation

## Abstract

The interactions between the atmosphere and the land surface are characterized by complex, non-linear processes on varying time scales. The Noah-MP is a medium complexity land-surface model (LSM), which was recently selected as the new default LSM for the hydrologically enhanced Weather Research and Forecasting modelling system (WRF-Hydro). Compared to its predecessor, several parameterizations were considerably improved and new ones added, inter alia more sophisticated groundwater descriptions, which aim to replace the traditional free-drainage lower boundary condition. This study investigates the benefits that can be obtained from a two-dimensional groundwater representation within the WRF-Hydro modelling system by performing two offline simulations for the upper Danube river basin. In comparison to the free-drainage reference simulation, the lateral routing of groundwater and the two-way interaction with the water table greatly enhances small scale variability in simulated fields of soil moisture content and evapotranspiration (ET). The representation of upward fluxes from the aquifer helps to maintain higher soil moisture contents and thus ET during prolonged dry periods. These differences are rather small though (<2%) and explained by the fact that the study region is considered to be limited by radiative energy and not water availability. The most striking difference however is the performance gap in simulating streamflow. WRF-Hydro with 2d groundwater scheme clearly outperforms the reference simulation in terms of performance metrics. A comparison with hourly streamflow observations for the water year of 2016 yields average Kling-Gupta efficiencies of 0.79 versus 0.57 for the reference. Given that both model configurations were not calibrated beforehand, we conclude that the two-dimensional groundwater option is especially beneficial for applications in poorly or even ungauged catchments. Furthermore, the inclusion of a so far missing compartment of the water cycle in the WRF-Hydro modelling system allows for a more holistic representation of interactions between atmosphere land surface and subsurface, which will be advantageous in feedback studies with the fully coupled WRF-Hydro.

**KEYWORDS**
free drainage, groundwater, land-surface model, WRF-hydro

# 1 | INTRODUCTION

Besides representations for atmosphere, oceans, and cryosphere, land surface schemes are an integral part in models describing the earth system on a global or regional scale. More precisely, they are providing the lower boundary to an atmospheric model by representing a variety of hydrological, biogeophysical, and biogeochemical processes and thus information on fluxes of heat, moisture, and momentum to the atmospheric model. Taking this background into account, many of the land surface models (LSMs) were originally developed with the coupled application in focus. Consequently, these models were aligned to the spatial resolutions commonly used by atmospheric models and are limited to a one-dimensional approach in describing vertical fluxes across the compartmental interfaces. Another characteristic—contrarily to classical hydrological models—is the fact that process descriptions with relevance for the fluxes at the upper boundary are typically more detailed than those of the lower boundary, that is, the bottom of the simulated soil column in a depth of 2-10 m (Wood et al., 2011).

One aspect of past and present endeavours to further evolve LSMs is the improvement of hydrological process descriptions within these model systems (e.g. Clark et al., 2015; Ning et al., 2019). The underlying motivation is mainly to achieve a better understanding of the interactions between the different compartments of the hydrological cycle, and thus to ultimately improve the results obtained from coupled applications, like weather and climate predictions. These interactions are currently far from being understood, as shown by the still growing number of studies investigating feedback mechanisms between the land-surface and the atmosphere (e.g. Arnault et al., 2016; Arnault et al., 2018; Arnault et al., 2019; Barlage et al., 2015; Davison et al., 2015; Fersch, Francke, et al., 2020; Forrester & Maxwell, 2020; Keune et al., 2016; Larsen et al., 2016; Rahman et al., 2015; Rummler et al., 2018; Senatore et al., 2015; Zhang et al., 2019).

In this regard, various efforts have been made to replace the crude, unidirectional, free-drainage boundary condition commonly found at the lower boundary of a typical LSM. More realistic descriptions were added that allowed for two-way interactions between the unsaturated zone and the water table. This led to a range of groundwater implementations with varying degrees of complexity and specific use cases in mind. These include one-dimensional, column-based approaches (e.g. Liang et al., 2003; Niu et al., 2005; Niu et al., 2007; Yeh & Eltahir, 2005) that are computationally very efficient and hence can be easily applied on a global scale. Medium complexity schemes additionally consider lateral flow between neighbouring grid-cells (e.g. Batelis et al., 2020; Miguez-Macho et al., 2007; Vergnes & Decharme, 2012) and have shown their applicability on continental and global scales in various studies using offline and fully coupled model configurations (e.g. Anyah et al., 2008; Barlage et al., 2015; Decharme et al., 2019; Fan et al., 2007; Martinez et al., 2016; Miguez-Macho & Fan, 2012). Three-dimensional variably saturated groundwater models like for example ParFlow (Ashby & Falgout, 1996) have also been integrated into LSMs (e.g. Kollet & Maxwell, 2006; Maxwell & Miller, 2005) and subsequently coupled to multiple

regional climate models (e.g. Maxwell et al., 2007; Maxwell et al., 2011; Shrestha et al., 2014; Sulis et al., 2017). Even though these models are considerably more expensive from a computational point of view, first applications on a continental scale (e.g. Keune et al., 2016; Maxwell et al., 2015) proved the basic feasibility of such endeavours.

In general, the evaluation of simulations with hydrologically enhanced LSMs showed that connecting the soil column of a LSM with the water table can lead to (1) a more realistic topographically-driven soil moisture distribution (e.g. Forrester & Maxwell, 2020; Larsen et al., 2016; Maxwell et al., 2007; Seuffert et al., 2002; Wagner et al., 2016), (2) an increase in soil moisture in areas with shallow water tables, which in turn (3) increases evapotranspiration in areas that are not energy-limited (e.g. Koirala et al., 2014; Kollet & Maxwell, 2006; Lam et al., 2011; Leung et al., 2010; Martinez et al., 2016) and (4) impacts runoff generation (e.g. Batelis et al., 2020; Koirala et al., 2014; Niu et al., 2007; Yeh & Eltahir, 2005).

However, hydrologically enhanced LSMs are not only used in process studies or coupled applications as outlined above, but also advance into areas that were previously covered by classical hydrological models, like flood forecasting (e.g. Givati et al., 2016). Recently, the WRF-Hydro modelling framework (Gochis et al., 2018) was selected to become the National Water Model (NWM) to provide streamflow forecasts over the entire continental United States. The coupling framework extends a traditional LSM with a range of modular hydrological physics options and a subgrid approach to account for example topographic heterogeneity. Groundwater processes, on the other hand, are currently represented in a comparatively simplistic way. This, however, shows the necessity to investigate the added value of an explicit two-dimensional groundwater parameterization within the WRF-Hydro modelling system, from which our research questions arise: How does the implementation of an explicit two-dimensional groundwater parameterization in the WRF-Hydro modelling system impact simulated variables of (i) soil moisture, (ii) evapotranspiration, and does it improve the model's skill in reproducing observed (iii) river streamflow? To answer these questions, we implement the groundwater scheme described in Miguez-Macho et al. (2007) into the WRF-Hydro modelling system and compare results from a simulation with explicit groundwater to those obtained from a simulation using the free-drainage boundary condition, which is currently the default option in both WRF-Hydro and the NWM.

# 2 | MODEL DESCRIPTION

## 2.1 | WRF-Hydro modelling system

WRF-Hydro version 5.1.1 (Gochis et al., 2020) is used as the hydrological model for this study. At its core, WRF-Hydro is a coupling framework that enhances a traditional one-dimensional land surface parameterization by providing additional descriptions for a range of hydrological processes, that is, representations for surface overland flow, saturated subsurface flow, channel routing, baseflow processes, and lakes or reservoirs. Since the typical grid scales, LSMs operate on

are too coarse to accurately route water across the landscape, WRF-Hydro uses a sub-grid approach to account for topographic heterogeneity. The model can be used as a traditional hydrological model, which is often referred to as "one-way coupling", "offline", or "standalone" mode, where the meteorological forcing data has to be supplied as gridded datasets. Alternatively, the model can be run in a fully coupled configuration, where the LSM constantly exchanges information with a limited area atmospheric model. The latter is driven by meteorological forcing at the lateral boundaries of the model domain and thus no additional hydrometeorological inputs to the LSM are required. This configuration is often referred to as "fully" or "two-way" coupled mode.

The default LSM since WRF-Hydro version 5 is the Noah-MP, which is an augmented Noah-LSM with Multi-Parameterization options (Niu et al., 2011; Yang et al., 2011). It is largely based on its predecessor (Noah-LSM), although changes to the code structure required a complete rewrite of the model code, which now follows a modular concept. Compared to the legacy Noah LSM, the range of user-selectable process descriptions has been considerably extended, like for example by the Ball-Berry canopy stomatal resistance scheme (Ball et al., 1987), a representation of dynamic vegetation (Dickinson et al., 1998), a multi-layer snowpack parameterization (Yang & Niu, 2003) with a more permeable frozen soil scheme (Niu & Yang, 2006), and several new runoff/groundwater options (e.g. Miguez-Macho et al., 2007; Niu et al., 2007). The soil column in the Noah-MP LSM has a fixed 2-m profile that is subdivided into four layers with thicknesses of 10, 30, 60, and 100 cm, respectively (Figure 1). Soil related model parameters are a function of textural class and read in from a lookup table.

## 2.2 | Free drainage runoff parameterization

The default runoff option in the WRF-Hydro model system is Noah-MP's free drainage condition (from now on referred to as FD), where simulated runoff is primarily governed by the three global parameters
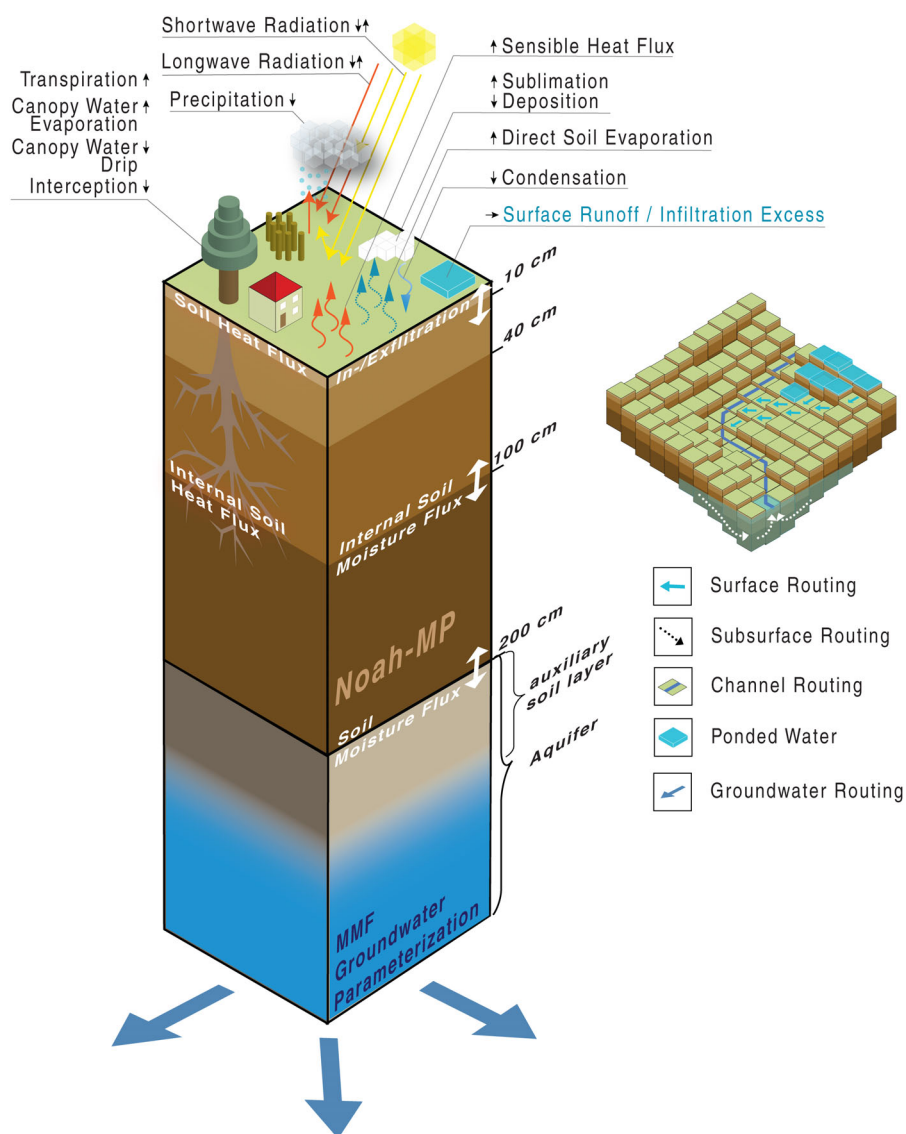


**FIGURE 1** A schematic illustration of a single soil column from the Noah-MP LSM with MMF groundwater parameterization (left) and the associated WRF-hydro routing extensions (right). Adapted from Rummler et al. (2018)

REFKDT, REFDK, and SLOPE (e.g. Yucel, Onen, Yilmaz, & Gochis, 2015; Cuntz et al., 2016). The first two parameters REFKDT (.) and REFDK (.) are infiltration scaling parameters that are used to determine the surface runoff $Q_{surface}$:

$$Q_{surface} = Q_{wat} - I_{max} \qquad (1)$$

where $Q_{wat}$ (m s$^{-1}$) is the water input rate on the soil surface, and $I_{max}$ (m s$^{-1}$) the soil infiltration rate, which is calculated as following:

$$I_{max} = Q_{wat} \frac{D[1 - \exp(-kdt \cdot \delta_t)]}{Q_{wat} + D[1 - \exp(-kdt \cdot \delta_t)]} \qquad (2)$$

with

$$D = \sum_{i=1}^{4} \Delta Z_i (\theta_{sat} - \theta_i) \qquad (3)$$

and

$$kdt = kdt_{ref} \cdot \frac{K_{sat}}{K_{ref}} \qquad (4)$$

where D (m) is the liquid soil moisture deficit of the modelled soil column, $\delta_t$ the time between two model time steps, Ksat (m s$^{-1}$) is the saturated hydraulic conductivity, Kref (m s$^{-1}$) the reference value for the saturated hydraulic conductivity (REFDK), which defaults to the value of the silty-clay-loam soil texture ($2 \times 10-6$ m s$^{-1}$) and kdtref the REFKDT parameter. Finally, the SLOPE parameter is a scaling factor moderating the percolation Qperc (mm):

$$Q_{perc} = Slope \cdot K_4 \qquad (5)$$

where $K_4$ (mm) is the drainage from the bottom soil layer, and *Slope* (.) is a scaling factor. By default, the Noah-MP LSM assumes a global *Slope* value of 0.1. When using WRF-Hydro's conceptual groundwater bucket option, $Q_{perc}$ is collected in those buckets and subsequently redistributed to the channel network. Groundwater buckets are user-definable and typically setup to cover the catchment area of individual river reaches or measurement locations.

## 2.3 | MMF runoff parameterization

Another, more complex, runoff option within the Noah-MP LSM is the two-dimensional MMF groundwater parameterization (Barlage et al., 2015; Fan et al., 2007; Miguez-Macho et al., 2007), which complements a traditional LSM by adding process descriptions for an unconfined aquifer. The interaction with the four soil layers of the LSM is accomplished by introducing an auxiliary soil layer with similar properties, which connects the bottommost 4th soil layer of the Noah-MP to the water table. The height of this additional layer can change over time and location via the means of vertical

and lateral water movement. Similar to the Noah-MP, vertical water movement within the unsaturated zone (i.e. drainage and capillary rise) is described using a one-dimensional form of the Richard's equation. Lateral water movement in the saturated zone follows Darcy's law and is described by the Dupuit–Forchheimer approximations, which relate the slope of the water table to groundwater flux. Storage changes $\Delta S$ (m) within the deep layer are given as:

$$\Delta S = \text{Recharge} + Q_{lateral} - Q_{river} \qquad (6)$$

with Recharge (m) being the flux to/from the 4th soil layer of the Noah-MP, $Q_{lateral}$ (m) being the sum of positive/negative fluxes to / from a grid cell and $Q_{river}$ (m) representing the groundwater flow to rivers:

$$Q_{river} = R_{cond} \cdot (h - z_{riverbed}) \qquad (7)$$

with $R_{cond}$ being the river conductivity (.), h the water table head (m), and $z_{riverbed}$ (m) the elevation of the assumed riverbed within a model grid cell. It is important to note that $Q_{river}$ is one-way only, so that fluxes from the riverbed to the groundwater are neglected.

The calculation of surface runoff differs from the one used by the default FD option (Equation 1). It is based on a TOPMODEL approach (Niu et al., 2005; Niu et al., 2011), describing the saturation excess of a fractionally saturated model grid cell, which is calculated by:

$$Q_{surface} = Q_{wat} \cdot ((1 - FCR_1) \cdot F_{sat} + FCR_1) \qquad (8)$$

with $FCR_1$ being the impermeable pore space fraction due to frozen soil within the 1st soil layer. The saturated surface fraction $F_{sat}$ is an exponential function of the depth to the water table and is calculated by:

$$F_{sat} = F_{max} \cdot e^{-0.5 \cdot f \cdot \max(z_{wt} - 2, \, 0)} \qquad (9)$$

with $f$ (m$^{-1}$) being a runoff decay factor with a hardcoded value of 6 m$^{-1}$, $z_{wt}$ (m) the depth to the water table, and $F_{max}$ (.) a tunable global runoff parameter, which represents the maximum saturated surface fraction of a model grid cell and defaults to a value of 0.38 within the Noah-MP. Thus, $F_{sat}$ becomes $F_{max}$ when $z_{wt}$ is within the resolved layers of the LSM, that is, $z_{wt} \leq 2$ m. Finally, the change in depth of the water table can be computed by:

$$\Delta z_{wt} = \frac{\Delta S}{(\theta_{sat} - \theta_{equ})} \qquad (10)$$

with $\Theta_{sat}$ (m$^3$ m$^{-3}$) and $\Theta_{equ}$ (m$^3$ m$^{-3}$) being the saturated and equilibrium soil moisture content, respectively. In case that $\Delta S$ is greater than the available pore space of the auxiliary layer, the water table can rise to soil layers of the LSM. If these layers get saturated before $\Delta S$ is fully depleted, the excess amount is treated as spring discharge $Q_{spring}$.

It is noted that values for $\Theta_{equ}$, $R_{cond}$, and $z_{riverbed}$ are computed during the initialization of the MMF parameterization via an internal spin-up routine. This routine requires an additional dataset on climatological groundwater recharge, which is provided by the WRF preprocessing system. For continental domains, the water table depth at $\Theta_{equ}$ is considered as the lateral boundary condition. For a more in-depth description of the MMF parameterization, the interested reader is referred to the descriptions given, for example, in Miguez-Macho et al. (2007), Fan and Miguez-Macho (2010), or Zhang et al. (2020).

## 2.4 | Model adjustments

The current implementation of the MMF groundwater option within the Noah-MP LSM relies on the parallelization infrastructure provided by the Weather Research and Forecast (WRF) atmospheric model (Skamarock et al., 2019). To make use of the parameterization in the offline variant of WRF-Hydro, the relevant code passages had to be adapted accordingly. Furthermore, the MMF scheme was not originally designed to accommodate for WRF-Hydro's routing extensions and vice versa. Hence, we made arrangements to incorporate $Q_{river}$ and $Q_{spring}$ within WRF-Hydro's coupling/routing concept. In particular, $Q_{river}$ is now redistributed to individual river reaches via the associated groundwater buckets and $Q_{spring}$ is added to the infiltration excess to make it available for redistribution with WRF-Hydro's surface routing scheme. A schematic overview of the MMF parameterization within the Noah-MP and WRF-Hydro's routing extensions is given Figure 1.

## 3 | STUDY REGION AND MODEL SETUP

### 3.1 | Study region and period/observations

We apply the WRF-Hydro model to the upper Danube river basin, with the outlet being located where the Danube crosses the border from Germany to Austria. The watershed has a total drainage area of 76 642 km² (Figure 2), with elevations ranging from 4049 to 286 m a. s.l. at the outlet. In general, the climate of the study region can be characterized as cool temperate and humid. Yearly average temperatures range from 9.5 degrees centigrade in the northern lower areas to subzero values in the glaciated alpine areas. Yearly mean precipitation amounts strongly depend on the location and can reach values well beyond 2400 mm/yr in the higher elevations of the northern alpine front range, whereas regions in the northern part of the study region or inner alpine valleys can receive amounts as low as 600 mm/yr. On average, the month with the highest precipitation amounts is typically July and 30%-40% of annual precipitation falls during the summer months. Exceptions to this rule are the low mountain ranges like the Upper-Palatine or Bavarian Forest where the precipitation maximum is usually found in December.

Geological units include from north to south the South German Scarplands, North Alpine Molasse Basin, folded Molasse zone,



**FIGURE 2** Elevation model of the WRF-hydro model domain. The channel network of the study region is shown as blue solid lines for channels with a stream order greater or equal to three. The elevation in meters above mean sea level is depicted by the colorbar on the left. The four catchments for which simulated streamflow is evaluated are marked by a red outline: (a) river Iller till gauge Kempten, (b) river Mangfall till gauge Rosenheim, (c) river Wörnitz till gauge Harburg, and (d) river Naab till gauge Münchshofen
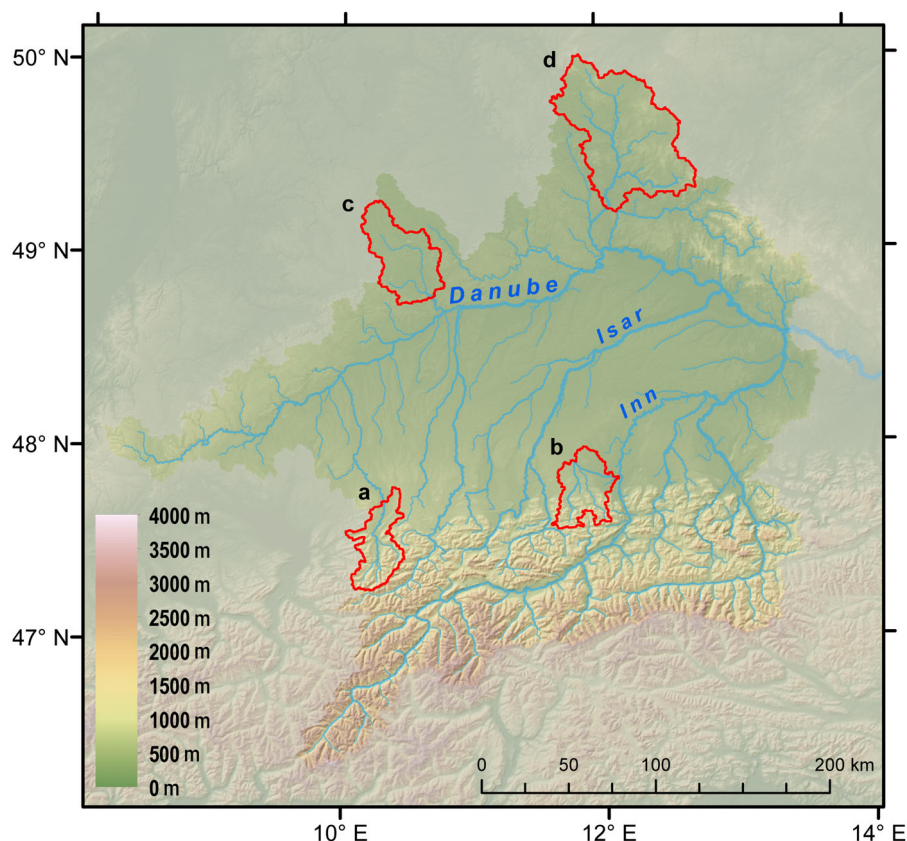
Helvetic zone, Flysch zone, Northern Limestone Alps, Alpine Gray-wacke, and the Austroalpine basement rocks. The rump of a mountain chain found in the eastern and north-eastern parts of the domain is characterized by metamorphic and magmatic basement rocks that were formed during variscan orogeny.

Highly productive fissured aquifers are found along the Northern Limestone Alps, as well as the Swabian and Franconian Jura north of the river Danube. Practically non-aquiferous rocks are located to the east and northeast of the river Danube and south of the river Inn (southern part of the domain). In the pre-alpine environment, conditions are heterogenous: highly productive porous aquifers are typically encountered in valley floors filled with quaternary river gravels, whereas low productive aquifers are found in areas with glacial moraine deposits and basin sediments.

The dominant land use class within the study region is cropland, occupying nearly 50% of the area, followed by needleleaf forests (22%) and mixed forests (8%). Soils in the study region are spatially highly variable, with the majority of soils having been developed in glacial, periglacial, or quaternary overburden layers. The dominant topsoil textural class within the study region is silt loam (37%), followed by loam (26%) and sandy loam (15%).

The water year 2016 was chosen as the study period. It should be noted that the temporal delimitation of a water year may vary slightly by country. Here, we follow the definition used, for example, by the United States Geological Survey and investigate the period between 1 October 2015 and 30 September 2016. In terms of precipitation amounts, the total amounts of the water year 2016 were close to the long-term average. The first three months of the study period were characterized by precipitation amounts below the long-term average. The second quarter of the water year started with substantial rainfall amounts in January and February that were well above the long-term average. In May and June, a series of strong convective precipitation events lead to localized flooding. In terms of temperature, the winter months were considerably warmer than the long-term average. Spring, on the other hand, was close to average and summer only slightly warmer.

## 3.2 | Experiment design and model setup

To assess the added value of a more detailed groundwater description within the WRF-Hydro modelling system, two experiments with the two runoff parameterizations outlined in Section 2.1 (FD) and Section 2.2 (MMF) are conducted. Both experiments use the model domain as shown in Figure 2, which has an extent of $460 \times 450$ km and spans the catchment of the upper Danube with a spatial resolution of 1 km. The WRF-Hydro routing extensions run on a sub-grid with the same extent, but a spatial resolution of 200 m, resulting in an aggregation factor of 5. The necessary high-resolution routing fields were derived from elevation data extracted from the EU-DEM (European Environment Agency, 2018). The drainage network was compared to the EU-Hydro river network database (European Environment Agency, 2019) to verify accuracy. In case of deviations with

respect to third- or higher-order channels, model topography was reconditioned so that flow directions resembled the observed ones. The initiation thresholds of first order channels were chosen in a way that the resulting drainage network density is close to the one of the reference dataset. The land use information is based on the CORINE dataset (Büttner & Kosztra, 2007), which was re-indexed to the classification system introduced by the International Geosphere Biosphere Program. The topsoil texture data is generated by merging datasets from the European Soil Database (Panagos et al., 2012) with information extracted from the Harmonized World Soil Database (Fischer et al., 2008).

The surface, subsurface and channel routing modules of WRF-Hydro are all activated for both experiments and executed with a time step of 15 s. The channel routing is done on a vectorized river network using the Muskingum-Cunge option. WRF-Hydro's conceptual groundwater bucket model is activated with the pass-through option for both experiments, so that water entering the bucket is immediately redistributed to the associated river reaches. In the FD experiment, the buckets receive input via percolation from the fourth soil layer (Equation 5), while in the MMF experiment the buckets are only used to redistribute water amounts originating from $Q_{river}$ (Equation 7). All other parametrization options in the Noah-MP are kept to the settings prescribed by WRF-Hydro's default configuration. Furthermore, it is important to note that the model calibration was limited to WRF-Hydro's channel network. To be more precise, only the settings for channel geometry and Manning's roughness coefficients were adjusted, based on results obtained from previous simulations (not shown). We opted for this approach to avoid issues introduced by overfitting model parameters, which would considerably limit the robustness of the results and thus statements on their transferability. We therefore neglect parameter and data uncertainty in this study and instead solely focus on the structural model uncertainty.

To assess the performance of the two runoff options, we employ a regional approach and compare simulated hourly streamflow to quality-controlled observations obtained from the state measurement network. Nash-Sutcliffe efficiency (NSE; Nash & Sutcliffe, 1970), Kling-Gupta efficiency (KGE; Gupta et al., 2009), and percent bias (PBIAS) are used as performance measures. As outlined by Prentice et al. (2015), streamflow can be seen as the residual of the water balance components precipitation, evapotranspiration, and storage changes and is thus considered to be a well-suited integrative measure. In this regard, a special focus is put on two left- and two right-hand tributaries of the Danube, whose catchments are shown in Figure 2a,b and properties are summarized in Table 1. This selection has been made to assess the model performance over a broader spectrum of natural physiogeographic characteristics and to honour the fact that the main mechanisms for high-flow events are inherently different for right- and left-hand tributaries of the Danube: Flood events in the southern (pre-) alpine catchments predominantly occur during the spring and summer months and are typically caused by high precipitations amounts in conjunction with a snow melt phase. Conversely, high-flow events in the northern tributaries are typically

**TABLE 1** Key characteristics of the four study catchments

| River/gauge | Catchment size | Average slope | Annual mean temperature range (Avg.) | Annual mean precipitation |
|---|---|---|---|---|
| Iller/Kempten | 955 km$^2$ | 25.3% | 0.2–8.2 (6.0) °C | 1922 mm |
| Mangfall/Rosenheim | 1095 km$^2$ | 13.9% | 2.9–9.4 (7.7) °C | 1526 mm |
| Wörnitz/Harburg | 1570 km$^2$ | 3.9% | 8.1–9.4 (8.9) °C | 750 mm |
| Naab/Münchshofen | 4009 km$^2$ | 5.7% | 5.5–9.2 (8.2) °C | 788 mm |

*Note*: Values for long-term annual mean temperature and precipitation were derived from gridded observational datasets provided by the German meteorological service.

found during the winter months, caused by high surface runoff amounts due to liquid precipitation falling onto saturated or frozen soil.

Since the focus of this study is on the added value of increased model complexity instead of investigating potential interactions between land-surface and atmosphere, the offline or one-way coupled WRF-Hydro is applied. This basically assures identical meteorological boundary conditions for both experiments and thus allows for a fair comparison of model results. The initial conditions for both experiments are taken from a spin-up run (water year 2012) that was cycled 100 times to account for the slow groundwater component of the MMF parameterization. It is noted that the FD experiment lacks a groundwater component and thus model spin-up is much faster. However, to avoid the possibility of tainting the comparison of the FD and MMF experiments by effects originating from different initial conditions, we opted to initialize both experiments with identical initial conditions. Subsequently, both experiments are run for the water years 2013 to 2016 and evaluated for the water year of 2016. The extended spin-up of three years was chosen to grant both experiments sufficient time to reach their respective soil moisture equilibrium states. Anthropogenic influences, such as reservoirs, diversions, or groundwater pumping are not considered in the simulation setups. This circumstance was accounted for in the selection process of the four study catchments, so that simulated runoff can be more easily compared with the observations. The hourly gridded meteorological forcing data used to drive both experiments is described in the following section.

## 3.3 | Meteorological forcing dataset

The regional reanalysis Cosmo Rea6 (Bollmeyer et al., 2014) was chosen to provide the meteorological forcing to both offline WRF-Hydro model runs. The regional reanalysis is derived from ECMWF's ERA-Interim reanalysis dataset (Dee et al., 2011) by dynamical downscaling with the COnsortium for Small-Scale MOdelling (COSMO) limited-area model (Doms & Baldauf, 2013) of the German Meteorological Service (DWD). Apart from the lateral boundary forcing at a 3-h interval, the reanalysis system features the continuous nudging of observations, a snow analysis every 6 h and a daily analysis of soil moisture and sea surface temperatures. The output data are available on an hourly basis with a spatial resolution of approximately 6 km for continental Europe and currently covers the period from 1995 to 2019.

The resulting datasets are provided free of charge and are available via DWD's open data distribution points.

Due to the differences in horizontal resolution, the necessary forcing data consisting of precipitation, surface pressure, air temperature, specific humidity, short- and longwave radiation, and near-surface wind information was remapped to the horizontal resolution of the Noah-MP model grid. Fields for near-surface temperature, specific humidity, surface pressure, and shortwave radiation were additionally modified with respect to the topography of the model domains. In particular, surface pressure was adjusted by applying the barometric formula. Near surface temperatures were downscaled by considering a lapse rate of 0.64°C per 100 m change in elevation. Specific humidity information was first converted to relative humidity, subsequently interpolated to the model domain and reconverted to specific humidity, taking into account the previously downscaled values of surface pressure and near surface temperature. Finally, downwelling shortwave radiation was adjusted for slope and shading effects by applying the method found in the radiation driver of the WRF model.

In contrast to traditional forcing datasets, which are often generated from interpolated station measurements, this approach provides physically consistent information and is deemed superior for data sparse regions. However, uncertainties remain in terms of model biases (Kaiser-Weiss et al., 2019). Local bias introduced by complex topography has been addressed with the postprocessing outlined above.

## 4 | RESULTS

### 4.1 | Impact of the improved groundwater representation on simulated soil moisture patterns and dynamics

Figure 3 depicts the average annual column integrated soil moisture content for both experiments and their relative difference. Overall, the representation and lateral transport of groundwater in the MMF simulation ensures a substantial higher spatial heterogeneity in terms of soil moisture, with a clearly visible influence of topography (Figure 2). Consequently, the largest positive changes in soil moisture content are found in areas with topographic convergence (e.g. river valleys) with values up to 20%–50% higher than in the FD simulation. Drier conditions, on the other hand, are simulated in higher elevations and along ridges.
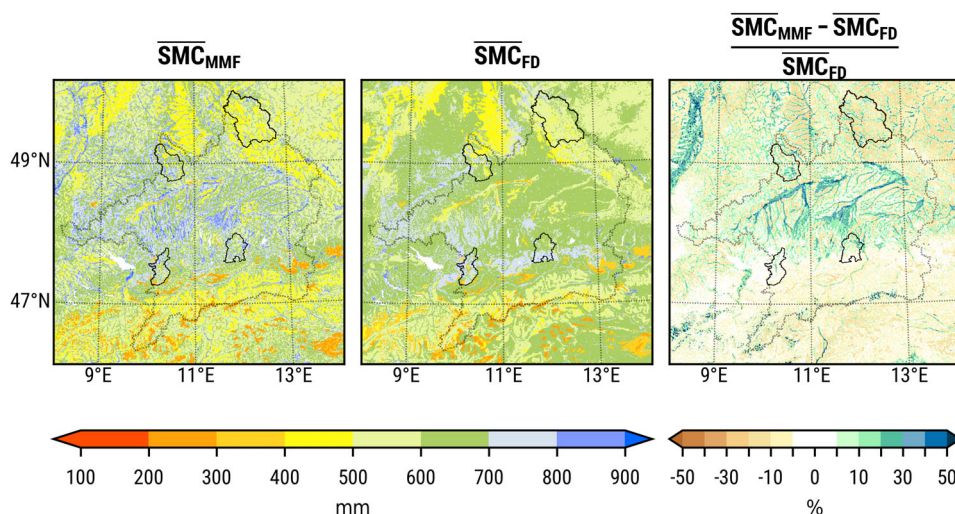
**FIGURE 3** (left and middle panel) Average column integrated soil moisture content (mm) for the water year 2016 and the simulations with two-dimensional groundwater parameterization (MMF) and free-drainage (FD) condition, respectively. (right panel) As in the left, except for the relative differences (%) between the MMF and FD experiment. The four study catchments are marked by black solid outlines and the basin of the upper Danube by a black dotted outline

The evolution of basin-averaged, column integrated soil saturation fraction for the four study catchments is shown in Figure 4. Across the board, the largest differences are found during the first months of the study period, where the MMF experiment maintains a higher soil saturation. This is thought to be related to a preceding drought that affected southern Germany during summer of 2015 and the subsequent months with precipitation amounts well below average. During this phase, the representation of groundwater—with the possibility to transport water upwards from the aquifer—is capable of maintaining higher soil moisture contents. The following months, however, show little differences, which is most likely related to the humid conditions with ample precipitation amounts and the fact that the FD experiment presented here uses the Noah-MP with the default scaling factor of 0.1 to constrain the percolation out of the bottommost soil layer (Equation 5). Additionally, both experiments employ WRF-Hydro's surface and subsurface routing modules, which allow for reinfiltration of surface runoff and therefore help to retain moisture within the model domain (e.g. Senatore et al., 2015; Yucel et al., 2015). This behaviour changes close to the end of the study period in August 2016, when the MMF experiment is again able to maintain wetter soils. An exception to this behaviour is the catchment of the river Woernitz, which shows lower values for most of the study period. This might be related to groundwater recharge and is further discussed in Section 4.3.

## 4.2 | Influence of the improved groundwater representation on simulated evapotranspiration patterns and dynamics

Figure 5 shows the annually averaged daily evapotranspiration (ET) for both experiments and their relative difference. Overall, a close resemblance to the changes in soil moisture (Figure 3, right) and thus topography can be recognized. Areas with high elevations (e.g. Alps in the south, Bavarian Forest in the north-east, or the Black Forest in the west of the domain) show overall little differences (± 5%), with the exception of those areas where the model resolution is high enough

to resolve individual valley structures, and the availability of sufficient quantities of energy to sustain a higher ET. Contrarily, ET is mostly unaffected by differences in soil moisture in the higher elevations, which can be explained by an energy deficit due to low temperatures and ample precipitation amounts. Spatially averaged values for ET are, on the other hand, very similar in both experiments. Averaged across the upper Danube basin (domain), the MMF experiment simulates values for ET that are 1.5% (0.5%) larger than in the FD experiment, which is on the order of soil moisture differences.

Shown in Figure 6 are the timeseries of catchment-averaged ET for the rivers Mangfall and Wörnitz. These two catchments have been selected due to the noticeable deviations in terms of soil moisture between the FD and MMF configuration at the beginning and the end of the study period, with lower soil saturation levels in the FD experiment (Figure 4b,c). In the Mangfall catchment, the impact of differences in soil moisture availability on ET is barely noticeable, which means that the soils are nevertheless still wet enough to not be a limiting factor for ET. The Wörnitz catchment, however, shows some deviation at the beginning of the timeseries in October and November of 2015, where the larger amounts of soil moisture in the MMF experiment exert a positive feedback on simulated ET. This is attributed to the unusual warm and dry weather conditions during that time period, as outlined in Section 4.2. The remaining time span, as well as the timeseries for the Iller and Naab catchments, show no noteworthy differences. Overall, from the watershed level up, the influence of the explicit groundwater parameterization on simulated ET is rather weak in this region.

## 4.3 | Ramifications of the improved groundwater representation on WRF-Hydro's streamflow prediction skill

The timeseries of simulated and observed hourly streamflow for the four study catchments are presented in Figure 7 and associated performance metrics in Table 2. Overall, the metrics obtained for the MMF experiment clearly outperform those of the FD experiment in all

FIGURE 4 Timeseries of basin-averaged soil saturation fraction (.) for the simulation with two-dimensional groundwater parameterization (MMF) and free-drainage (FD) condition, respectively. (a) River Iller till gauge Kempten, (b) river Mangfall till gauge Rosenheim, (c) river Wörnitz till gauge Harburg, and (d) river Naab till gauge Münchshofen
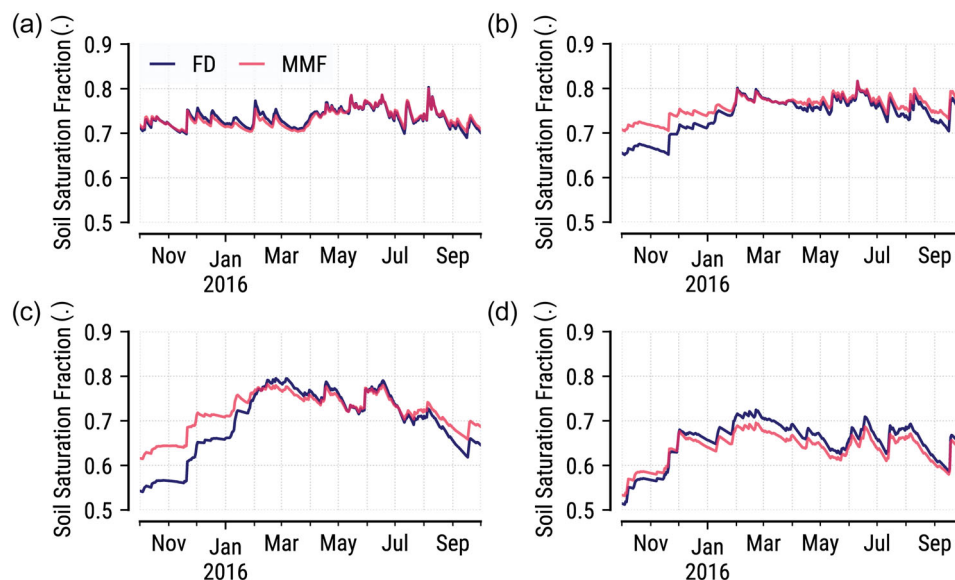


FIGURE 5 (left and middle panel) Average daily evapotranspiration (mm d$^{-1}$) for the water year 2016 and the simulation with two-dimensional groundwater parameterization (MMF) and free-drainage (FD) condition, respectively. (right panel) As in the left, except for the relative differences (%) between the MMF and FD experiment. The four study catchments are marked by black solid outlines and the basin of the upper Danube by a black dotted outline
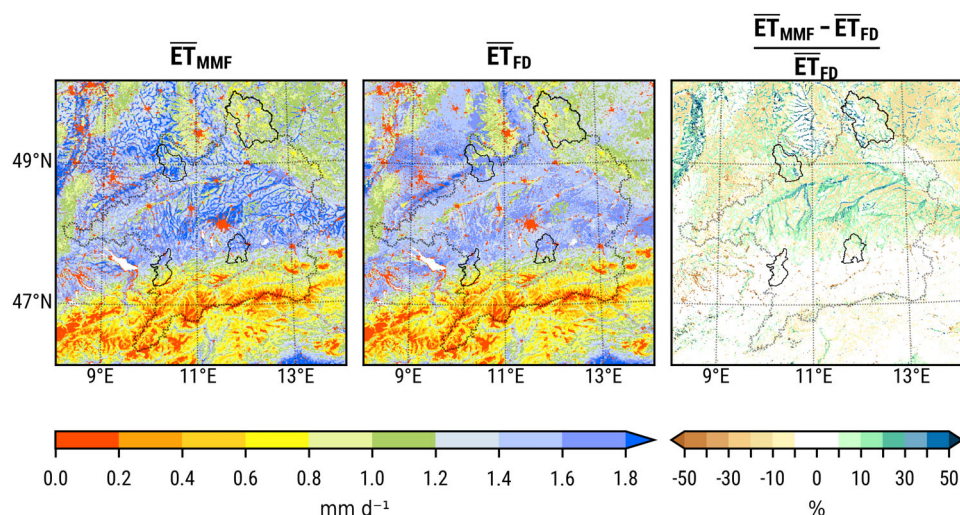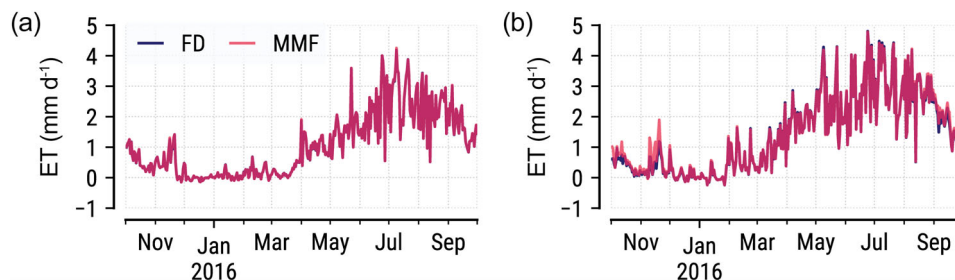


FIGURE 6 Timeseries of basin-averaged evapotranspiration (mm d$^{-1}$) for the simulation with two-dimensional groundwater parameterization (MMF) and free-drainage (FD) condition, respectively. (a) River Mangfall till gauge Rosenheim and (b) river Wörnitz till gauge Harburg



four study catchments and presented measures, with the exception of PBIAS in the Iller catchment. Most striking, however, is the fact that the performance difference between the FD and MMF simulation is considerably larger in the northern than in the southern study catchments.

Indeed, the southern study catchments receive considerable higher precipitation amounts (Table 1) and therefore the soil columns in the FD experiment are also more likely to reach the higher

saturation levels found with the MMF experiment (Figure 4a,b), which in turn might lead to more similar surface runoff amounts in response to a precipitation event. Additionally, the complex topography with steep slope angles (Figure 1 and Table 1) further favours fast runoff generation and lateral redistribution due to saturation excess overland flow and subsurface return flow. These processes are represented in both model configurations by WRF-Hydro's surface and subsurface routing capabilities, so the differences in simulated streamflow
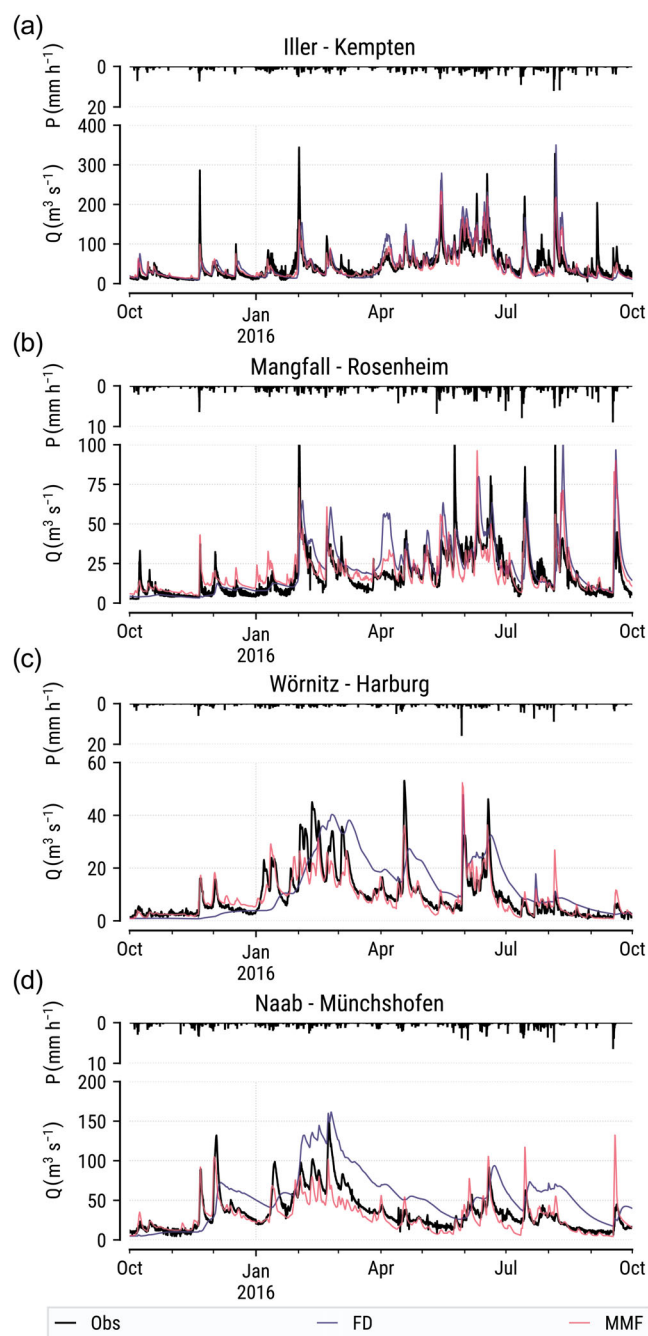
**FIGURE 7** Timeseries of hourly observed and simulated streamflow Q ($m^3 s^{-1}$) for the simulation with two-dimensional groundwater parameterization (MMF) and free-drainage (FD) condition, respectively. The observation (Obs) is shown as solid black line. A timeseries of basin-averaged precipitation P (mm h$^{-1}$) is shown in the upper part of each panel. (a) River Iller till gauge Kempten, (b) river Mangfall till gauge Rosenheim, (c) river Wörnitz till gauge Harburg, and (d) river Naab till gauge Münchshofen

As shown by the unsatisfactory NSE results with values of 0.12 and − 0.58, the FD experiment has serious difficulties with predicting the right timing and magnitude of peak flow events in the catchments of the rivers Wörnitz and Naab. In particular, a couple of events during the first three month of the study period are not captured at all (Figure 7c,d). This issue is absent or far less prominent in the MMF experiment, as showcased by the superior results in terms of performance metrics, for example, NSE of 0.72 and 0.62, respectively. The temporal delay of runoff peaks and the high values for PBIAS in case of the FD experiment suggests that there is too little surface runoff and, instead, too much infiltration and subsequently moisture leaving the model via percolation from the lowest soil layer. This assumption is additionally supported by the slightly higher soil saturation found in the FD simulation during spring and summer of 2016 (Figure 4c,d), and basin-averaged groundwater recharge amounts (Figure 8c,d) that roughly resemble the dynamics of simulated streamflow. It is noted that groundwater recharge means inflow to the groundwater bucket model of WRF-Hydro in the FD simulation context.

The MMF simulation, however, captures most of the peak flow events and is able to reasonably reproduce baseflow amounts as shown by KGE values of 0.8 and 0.76, respectively. The rather large negative PBIAS of −13.4% for the Naab catchment can be explained by excessive amounts of recharge (Figure 8d), which is consistent with the lower values for soil saturation fraction (Figure 4d) described in Section 4.1.

## 5 | DISCUSSION

The evaluation of simulated hourly streamflow at four different locations in the study region revealed that the simulation with groundwater representation was far more capable in capturing the dynamics, variability, and total amounts of observed hourly runoff amounts as shown by an average KGE of 0.79 versus 0.57. We contend that the higher heterogeneity in terms of soil moisture and the additional information on water table depth, which the MMF simulation employs in the calculation of infiltration excess amounts (Equations 8, 9), help to achieve a more realistic representation of runoff separation in fast, intermediate, and slow components within the WRF-Hydro model system. A similar improvement has been recently reported by Batelis et al. (2020), who implemented a 2D groundwater scheme in the Joint UK Land Environment Simulator. As shown by a series of previous WRF-Hydro modelling studies (e.g. Fersch, Senatore, et al., 2020; Kerandi et al., 2017; Lahmers et al., 2019; Yucel et al., 2015), the default (FD) model configuration typically requires calibration of the surface runoff (Equations 2, 3, 4) and percolation (s. Equation 5) parameters, among others, to adequately reproduce the observed runoff amounts.

The often-tedious task of calibrating the model to observed streamflow (e.g. Fersch et al., 2020a; Yin et al., 2020) is usually limited by computational constraints and bound to catchments with sufficient observational data, relying on the transferability of parameters for areas without observational data. For offline model applications with

between the two experiments are comparatively smaller in that environment.

In contrast, the situation in the northern study catchments is quite different. Both catchments receive substantially less precipitation, and the topography is less pronounced (s. Table 1 and Figure 1).

**TABLE 2** Performance metrics of simulated hourly streamflow with respect to gauge observations, for the water year 2016

| | NSE | | KGE | | PBIAS | |
|---|---|---|---|---|---|---|
| River / gauge | MMF | FD | MMF | FD | MMF | FD |
| Iller/Kempten | 0.69 | 0.33 | 0.84 | 0.69 | −4.8% | 3.8% |
| Mangfall/Rosenheim | 0.56 | 0.19 | 0.71 | 0.63 | 9.7% | 21.6% |
| Wörnitz/Harburg | 0.72 | 0.12 | 0.80 | 0.57 | −6.1% | 29.1% |
| Naab/Münchshofen | 0.62 | −0.58 | 0.76 | 0.37 | −13.4% | 56.8% |

*Note*: MMF and FD denotes the WRF-hydro simulation with two-dimensional groundwater parameterization and free-drainage condition, respectively.
Abbreviations: KGE, Kling-Gupta efficiency; NSE, Nash-Sutcliffe efficiency; PBIAS, percent bias.

**FIGURE 8** Timeseries of basin-averaged groundwater recharge (mm d$^{-1}$) for the simulation with two-dimensional groundwater parameterization (MMF) and free-drainage (FD) condition, respectively. Positive (negative) values represent downward (upward) fuxes. (a) River Iller till gauge Kempten, (b) river Mangfall till gauge Rosenheim, (c) river Wörnitz till gauge Harburg, (d) river Naab till gauge Münchshofen
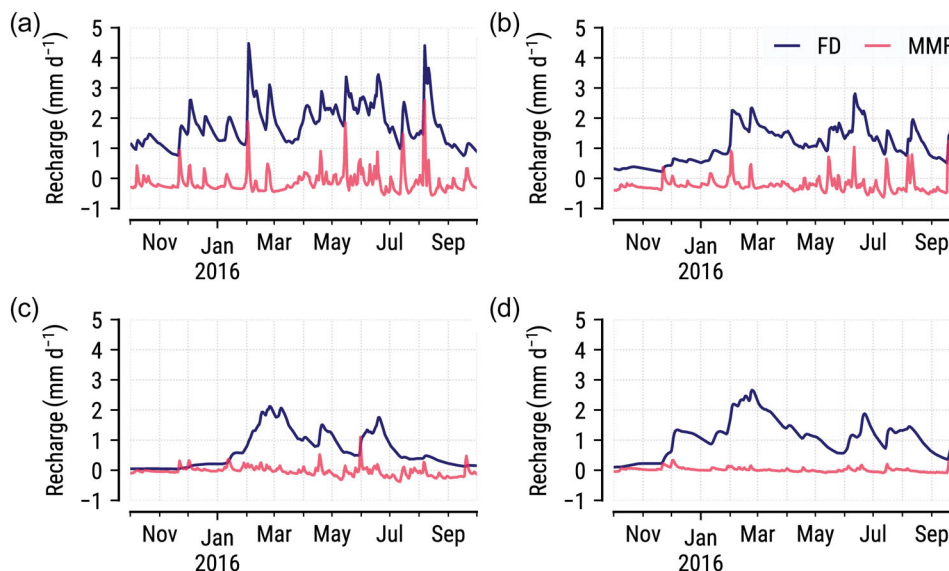


a focus on a limited area this is probably not critical. It becomes a concern, however, in fully coupled model applications, where the atmospheric model mandates a considerable minimum size of the model domain and feedbacks between land-surface and atmosphere are possible. Taking the results presented in this study into consideration, it can be assumed that a calibration of the FD model configuration would very likely yield different parameter settings for the northern and southern study catchments and thus limit their transferability. In contrast, the simulation with explicit groundwater representation has shown potential to achieve satisfactory values for example KGE with a reduced set of so far uncalibrated model parameters, which might make it a viable choice for applications in ungauged catchments and large model domains where model calibration is limited due to the constraints outlined above.

Compared to the baseline WRF-Hydro configuration, the simulation with MMF groundwater scheme increases the computational time by less than 5%, which would not add significantly to computational cost in long-term simulations. This is achieved by allowing for a series of simplifying assumptions in terms of model physics, as well as the structure and properties of the subsurface. Considering that the complexity of individual model components should be balanced (Prentice et al., 2015), we argue that the presented groundwater implementation is nevertheless a valuable addition to the WRF hydro-modelling system and usefully augments the already existing parameterizations for surface and subsurface routing. For more sophisticated application scenarios that for example demand for a variably saturated 3D representation of subsurface flow or a representation of human interaction through extraction of groundwater, one of the models presented in example Kollet et al. (2017) might be a more appropriate choice. Although at the cost of a considerable higher computational burden and additional data requirements (Rahman et al., 2019; Tijerina et al., 2021).

Results further demonstrated that a representation of lateral groundwater fluxes and two-way interactions between water table and soil column lead to a considerably higher spatial heterogeneity in terms of simulated soil moisture content and, to a somewhat lesser extent, evapotranspiration. Overall, a strong link to model topography was evident, which is in line with the findings of Forrester and Maxwell (2020) and Batelis et al. (2020). While a comparison on a point basis yielded considerable differences on the order of −30% to 50% for these quantities, the spatial averages for the study region (< 2%) and domain (< 1%) were very close. This can be attributed to the fact that the region is not water limited, but energy limited which is supported by analysis of long-term averaged climate datasets (Klingler et al., 2021).

The verification of the identified differences in simulated soil moisture content with observations, however, remains an open issue due to a lack of suitable observational datasets at intermediate scales

(Robinson et al., 2008). Considerable differences were identified along ridges and valley structures, while only subtle differences were obtained for catchment averages. This underlines the need for observational datasets that at least (a) cover an extent on the order of tens of kilometres and (b) provide the information at suitable spatial scales. In this context, a promising option might be the cosmic ray neuron sensing technique proposed by Zreda et al. (2008). The non-invasive measurement approach alleviates the representativeness issue of point measurements by having a measurement footprint on the order of hundreds of meters, which suits the resolutions typically used by LSMs. Measurement depths are superior to airborne or satellite-based remote sensing products and are on the order of tens of centimetres. Consequently, the method may have potential to also capture soil moisture content in the root zone, which is of crucial importance for plant transpiration. Additionally, mobile measurement equipment (Desilets et al., 2010) can be used to retrieve measurements with greater spatial detail for specific areas of interest, for example, valley transects where our simulations showed considerable differences. The measurement network presented in Fersch et al. (2020b), for example, could be a suitable starting point if a different strategy is used for the placement of sensors.

Finally, the results obtained for soil moisture bias and heterogeneity might also be relevant for further feedback studies with the fully coupled WRF-Hydro modelling system. As outlined by Wood et al. (2011), many warm-season precipitation events are thought to be potentially sensitive towards small-scale variabilities in land-surface properties, like for example topography, land-use and soil moisture. In particular, feedbacks are expected during the warm season and phases of weak synoptic forcing that allow for the development of mesoscale circulation (Taylor, 2015; Taylor et al., 2007). In terms of soil moisture, two mechanisms are conceivable: A positive feedback loop via the concept of precipitation recycling (e.g. Eltahir & Bras, 1996), which relates the contribution of local evapotranspiration to local precipitation. Alternatively, a negative feedback loop due to the location of convective initiation (Taylor, 2015; Baur, Keil, & Kraig, 2018). Differential heating of dry and moist patches is thought to create circulation cells within the planetary boundary layer, resulting in convergence over dry and divergence over wet patches. An increase of precipitation is thus obtained for the dry patches, since convergence supports an earlier transition from shallow to deep convection at those locations.

The findings of this study indicate that simulations with the MMF scheme may facilitate or strengthen positive feedback loops during prolonged dry phases, when the explicit groundwater representation can provide additional moisture to sustain higher evapotranspiration rates. In addition, the higher topography-induced heterogeneity of soil moisture simulated by the MMF scheme may enable or amplify negative feedback loops under favourable conditions.

## 6 | CONCLUSIONS

In this study, we replaced WRF-Hydro's empirical groundwater bucket model with a two-dimensional groundwater scheme and explored potential benefits of an explicit representation of a so far missing major compartment of the water cycle in the modelling system. The low additional computational cost and modest data requirements enable applications over large model domains—as typically found in fully coupled model setups—and over long time periods, such as the dynamical downscaling of climate scenarios. Results from a real-world application in the upper Danube catchment suggest that an explicit groundwater treatment can substantially improve the ability of the uncalibrated model to reproduce observed runoff volumes, which is particularly beneficial for model applications in poorly or even ungauged basins. The groundwater-enhanced model configuration exhibits a higher topographically-induced heterogeneity in soil moisture content and evapotranspiration, which lends itself to further investigation with the fully coupled modelling system to study potential feedbacks between soil moisture and precipitation. It is important to note, however, that the study region presented here is energy limited, which constrains the transferability of our results to other hydro-climatic regions and underlines the necessity of further model evaluation. Yet, the results of this study demonstrate that a better representation of groundwater is highly desirable in the current LSM of WRF-Hydro in particular and for LSMs with free drainage lower boundary condition in general.

## DATA AVAILABILITY STATEMENT

The model code and data that supports the findings of this study are available from the corresponding author upon reasonable request. The Cosmo Rea6 reanalysis dataset provided by the German meteorological service (DWD) can be obtained free of charge at: https://opendata.dwd.de/climate_environment/REA/COSMO_REA6/

## ORCID

*Thomas Rummler* https://orcid.org/0000-0001-7765-2275
*Joël Arnault* https://orcid.org/0000-0001-8859-5173

## REFERENCE

Anyah, R. O., Weaver, C. P., Miguez-Macho, G., Fan, Y., & Robock, A. (2008). Incorporating water table dynamics in climate modeling: 3. Simulated groundwater influence on coupled land-atmosphere variability. *Journal of Geophysical Research*, 113, 1–15.

Arnault, J., Rummler, T., Baur, F., Lerch, S., Wagner, S., Fersch, B., Zhang, Z., Kerandi, N., Keil, C., & Kunstmann, H. (2018). Precipitation

sensitivity to the uncertainty of terrestrial water flow in WRF-hydro: An ensemble analysis for Central Europe. *Journal of Hydrometeorology*, 19(6), 1007–1025. https://doi.org/10.1175/jhm-d-17-0042.1

Arnault, J., Wagner, S., Rummler, T., Fersch, B., Bliefernicht, J., Andresen, S., & Kunstmann, H. (2016). Role of runoff–infiltration partitioning and resolved overland flow on land–atmosphere feedbacks: A case study with the WRF-hydro coupled modeling system for West Africa. *Journal of Hydrometeorology*, 17, 1489–1516. https://doi.org/10.1175/JHM-D-15-0089.1

Arnault, J., Wei, J., Rummler, T., Fersch, B., Zhang, Z., Jung, G., Wagner, S., & Kunstmann, H. (2019). A joint soil-vegetation-atmospheric water tagging procedure with WRF-hydro: Implementation and application to the case of precipitation partitioning in the upper Danube River basin. *Water Resources Research*, 55(7), 6217–6243. https://doi.org/10.1029/2019wr024780

Ashby, S. F., & Falgout, R. D. (1996). A parallel multigrid preconditioned conjugate gradient algorithm for groundwater flow simulations. *Nuclear Science and Engineering*, 124(1), 145–159. https://doi.org/10.13182/nse96-a24230

Ball, J. T., Woodrow, I. E., & Berry, J. A. (1987). A model predicting stomatal conductance and its contribution to the control of photosynthesis under different environmental conditions. In *Progress in photosynthesis research* (pp. 221–224). Springer. https://doi.org/10.1007/978-94-017-0519-6_48

Barlage, M., Tewari, M., Chen, F., Miguez-Macho, G., Yang, Z.-L., & Niu, G.-Y. (2015). The effect of groundwater interaction in north American regional climate simulations with WRF/Noah-MP. *Climatic Change*, 129(3–4), 485–498. https://doi.org/10.1007/s10584-014-1308-8

Batelis, S.-C., Rahman, M., Kollet, S., Woods, R., & Rosolem, R. (2020). Towards the representation of groundwater in the joint UKland environment simulator. *Hydrological Processes*, 34(13), 2843–2863. https://doi.org/10.1002/hyp.13767

Baur, F., Keil, C., & Craig, G. C. (2018). Soil moisture–precipitation coupling over Central Europe: Interactions between surface anomalies at different scales and the dynamical implication. *Quarterly Journal of the Royal Meteorological Society*, 144(717), 2863–2875. https://doi.org/10.1002/qj.3415

Bollmeyer, C., Keller, J. D., Ohlwein, C., Wahl, S., Crewell, S., Friederichs, P., Hense, A., Keune, J., Kneifel, S., Pscheidt, I., Redl, S., & Steinke, S. (2014). Towards a high-resolution regional reanalysis for the European CORDEX domain. *Quarterly Journal of the Royal Meteorological Society*, 141(686), 1–15. https://doi.org/10.1002/qj.2486

Büttner, G. & Kosztra, B. (2007). *CLC2006 Technical guidelines. Technical Report 17. European Environment Agency*. http://www.eea.europa.eu/publications/technical_report_2007_17.

Clark, M. P., Nijssen, B., Lundquist, J. D., Kavetski, D., Rupp, D. E., Woods, R. A., Freer, J. E., Gutmann, E. D., Wood, A. W., Gochis, D. J., Rasmussen, R. M., Tarboton, D. G., Mahat, V., Flerchinger, G. N., & Marks, D. G. (2015). A unified approach for process-based hydrologic modeling: 2. Model implementation and case studies. *Water Resources Research*, 51(4), 2515–2542. https://doi.org/10.1002/2015wr017200

Cuntz, M., Mai, J., Samaniego, L., Clark, M., Wulfmeyer, V., Branch, O., Attinger, S., & Thober, S. (2016). The impact of standard and hard-coded parameters on the hydrologic fluxes in the Noah-MP land surface model. *Journal of Geophysical Research: Atmospheres*, 121(18), 10676–10700. https://doi.org/10.1002/2016jd025097

Davison, J. H., Hwang, H.-T., Sudicky, E. A., & Lin, J. C. (2015). Coupled atmospheric, land surface, and subsurface modeling: Exploring water and energy feedbacks in three-dimensions. *Advances in Water Resources*, 86, 73–85. https://doi.org/10.1016/j.advwatres.2015.09.002

Decharme, B., Delire, C., Minvielle, M., Colin, J., Vergnes, J.-P., Alias, A., Saint-Martin, D., Séférian, R., Sénési, S., & Voldoire, A. (2019). Recent changes in the ISBA-CTRIP land surface system for use in the CNRM-CM6 climate model and in global off-line hydrological applications. *Journal of Advances in Modeling Earth Systems*, 11(5), 1207–1252. https://doi.org/10.1029/2018ms001545

Dee, D. P., Uppala, S. M., Simmons, A. J., Berrisford, P., Poli, P., Kobayashi, S., Andrae, U., Balmaseda, M. A., Balsamo, G., Bauer, P., Bechtold, P., Beljaars, A. C. M., van de Berg, L., Bidlot, J., Bormann, N., Delsol, C., Dragani, R., Fuentes, M., Geer, A. J., … Vitart, F. (2011). The ERA-interim reanalysis: Configuration and performance of the data assimilation system. *Quarterly Journal of the Royal Meteorological Society*, 137, 553–597. https://doi.org/10.1002/qj.828

Desilets, D., Zreda, M., & Ferré, T. P. A. (2010). Natureneutron probe: Land surface hydrology at an elusive scale with cosmic rays. *Water Resources Research*, 46(11). https://doi.org/10.1029/2009wr008726

Dickinson, R. E., Shaikh, M., Bryant, R., & Graumlich, L. (1998). Interactive canopies for a climate model. *Journal of Climate*, 11(11), 2823–2836. https://doi.org/10.1175/1520-0442(1998)011<2823:icfacm>2.0.co;2

Doms, G. & Baldauf, M. (2013). COSMO-model version 5.00: A description of the nonhydrostatic regional COSMO-model—part I: Dynamics and numerics. https://doi.org/10.5676/DWD_PUB/NWV/COSMO-DOC_5.00_I

Eltahir, E. A. B., & Bras, R. L. (1996). Precipitation recycling. *Reviews of Geophysics*, 34(3), 367–378. https://doi.org/10.1029/96rg01927

European Environment Agency. (2018). *EU-DEM v1.1*. https://land.copernicus.eu/imagery-in-situ/eu-dem/eu-dem-v1.1

European Environment Agency. (2019). River network database, Version 1.3. https://land.copernicus.eu/imagery-in-situ/eu-hydro/eu-hydro-river-network-database

Fan, Y., & Miguez-Macho, G. (2010). Potential groundwater contribution to Amazon evapotranspiration. *Hydrology and Earth System Sciences*, 14(10), 2039–2056. https://doi.org/10.5194/hess-14-2039-2010

Fan, Y., Miguez-Macho, G., Weaver, C. P., Walko, R., & Robock, A. (2007). Incorporating water table dynamics in climate modeling: 1. Water table observations and equilibrium water table simulations. *Journal of Geophysical Research*, 112, D10125. https://doi.org/10.1029/2006JD008111

Fersch, B., Francke, T., Heistermann, M., Schrön, M., Döpper, V., Jakobi, J., Baroni, G., Blume, T., Bogena, H., Budach, C., Gränzig, T., Förster, M., Güntner, A., Franssen, H.-J. H., Kasner, M., Köhli, M., Kleinschmit, B., Kunstmann, H., Patil, A., … Oswald, S. (2020). A dense network of cosmic-ray neutron sensors for soil moisture observation in a highly instrumented pre-alpine headwater catchment in Germany. *Earth System Science Data*, 12(3), 2289–2309. https://doi.org/10.5194/essd-12-2289-2020

Fersch, B., Senatore, A., Adler, B., Arnault, J., Mauder, M., Schneider, K., Völksch, I., & Kunstmann, H. (2020). High-resolution fully coupled atmospheric–hydrological modeling: A cross-compartment regional water and energy cycle evaluation. *Hydrology and Earth System Sciences*, 24(5), 2457–2481. https://doi.org/10.5194/hess-24-2457-2020

Fischer, G., Nachtergaele, F., Prieler, S., van Velthuizen, H. T., Verelst, L., & Wiberg, D. (2008). *Global agro-ecological zones assessment for agriculture (GAEZ 2008)*. IIASA, Laxenburg, Austria and FAO, Rome, Italy.

Forrester, M. M., & Maxwell, R. M. (2020). Impact of lateral groundwater flow and subsurface lower boundary conditions on atmospheric boundary layer development over complex terrain. *Journal of Hydrometeorology*, 21(6), 1133–1160. https://doi.org/10.1175/jhm-d-19-0029.1

Givati, A., Gochis, D., Rummler, T., & Kunstmann, H. (2016). Comparing one-way and two way coupled hydrometeorological forecasting systems for flood forecasting in the Mediterranean region. *Hydrology*, 3, 19.

Gochis, D., Barlage, M., Cabell, R., Dugger, A., Fanfarillo, A., FitzGerald, K., McAllister, M., McCreight, J., RafieeiNasab, A., Read, L., Frazier, N., Johnson, D., Mattern, J. D., Karsten, L., Mills, T. J., & Fersch, B. (2020). WRF-Hydro® v5.1.1. Zenodo.

Gochis, D., Barlage, M., Dugger, A., FitzGerald, K., Karsten, L., McAllister, M., McCreight, J., Mills, J., RafieeiNasab, A., Read, L., Sampson, K., Yates, D., & Yu, W. (2018). The WRF-hydro modeling system technical description, (Version 5.0). (p. 107). NCAR Technical Note. https://ral.ucar.edu/sites/default/files/public/WRF-HydroV5TechnicalDescription.pdf

Gupta, H. V., Kling, H., Yilmaz, K. K., & Martinez, G. F. (2009). Decomposition of the mean squared error and NSE performance criteria: Implications for improving hydrological modelling. *Journal of Hydrology*, 377(1–2), 80–91. https://doi.org/10.1016/j.jhydrol.2009.08.003

Kaiser-Weiss, A. K., Borsche, M., Niermann, D., Kaspar, F., Lussana, C., Isotta, F. A., van den Besselaar, E., van der Schrier, G., & Undén, P. (2019). Added value of regional reanalyses for climatological applications. *Environmental Research Communications*, 1(7), 71004. https://doi.org/10.1088/2515-7620/ab2ec3

Kerandi, N., Arnault, J., Laux, P., Wagner, S., Kitheka, J., & Kunstmann, H. (2017). Joint atmospheric-terrestrial water balances for East Africa: A WRF-hydro case study for the upper Tana River basin. *Theoretical and Applied Climatology*, 131(3–4), 1337–1355. https://doi.org/10.1007/s00704-017-2050-8

Keune, J., Gasper, F., Goergen, K., Hense, A., Shrestha, P., Sulis, M., & Kollet, S. (2016). Studying the influence of groundwater representations on land surface-atmosphere feedbacks during the European heat wave in 2003. *Journal of Geophysical Research: Atmospheres*, 121(22), 13301–13325. https://doi.org/10.1002/2016jd025426

Klingler, C., Schulz, K., & Herrnegger, M. (2021). Lamah-CE: large-sample data for hydrology and environmental sciences for central europe. *Earth System Science Data*, 13(9), 4529–4565. https://doi.org/10.5194/essd-13-4529-2021

Koirala, S., Yeh, P. J.-F., Hirabayashi, Y., Kanae, S., & Oki, T. (2014). Global-scale land surface hydrologic modeling with the representation of water table dynamics. *Journal of Geophysical Research: Atmospheres*, 119(1), 75–89. https://doi.org/10.1002/2013jd020398

Kollet, S. J., & Maxwell, R. M. (2006). Integrated surface–groundwater flow modeling: A free-surface overland flow boundary condition in a parallel groundwater flow model. *Advances in Water Resources*, 29(7), 945–958. https://doi.org/10.1016/j.advwatres.2005.08.006

Kollet, S., Sulis, M., Maxwell, R. M., Paniconi, C., Putti, M., Bertoldi, G., Coon, E. T., Cordano, E., Endrizzi, S., Kikinzon, E., Mouche, E., Mügler, C., Park, Y.-J., Refsgaard, J. C., Stisen, S., & Sudicky, E. (2017). The integrated hydrologic model intercomparison project, IH-MIP2: A second set of benchmark results to diagnose integrated hydrology and feedbacks. *Water Resources Research*, 53(1), 867–890. https://doi.org/10.1002/2016wr019191

Lahmers, T. M., Gupta, H., Castro, C. L., Gochis, D. J., Yates, D., Dugger, A., Goodrich, D., & Hazenberg, P. (2019). Enhancing the structure of the WRF-hydro hydrologic model for semiarid environments. *Journal of Hydrometeorology*, 20(4), 691–714. https://doi.org/10.1175/jhm-d-18-0064.1

Lam, A., Karssenberg, D., van den Hurk, B. J. J. M., & Bierkens, M. F. P. (2011). Spatial and temporal connections in groundwater contribution to evaporation. *Hydrology and Earth System Sciences*, 15(8), 2621–2630. https://doi.org/10.5194/hess-15-2621-2011

Larsen, M. A. D., Højmark Rasmussen, S., Drews, M., Butts, M. B., Christensen, J. H., & Refsgaard, J. C. (2016). Assessing the influence of groundwater and land surface scheme in the modelling of land surface-atmosphere feedbacks over the FIFE area in Kansas, USA. *Environmental Earth Sciences*, 75, 130. https://doi.org/10.1007/s12665-015-4919-0

Leung, L. R., Huang, M., Qian, Y., & Liang, X. (2010). Climate–soil–vegetation control on groundwater table dynamics and its feedbacks in a climate model. *Climate Dynamics*, 36, 57–81.

Liang, X., Xie, Z., & Huang, M. (2003). A new parameterization for surface and groundwater interactions and its impact on water budgets with the variable infiltration capacity (VIC) land surface model. *Journal of Geophysical Research*, 108(D16). https://doi.org/10.1029/2002jd003090

Martinez, J. A., Dominguez, F., & Miguez-Macho, G. (2016). Effects of a groundwater scheme on the simulation of soil moisture and evapotranspiration over southern South America. *Journal of Hydrometeorology*, 17(11), 2941–2957. https://doi.org/10.1175/jhm-d-16-0051.1

Maxwell, R. M., Chow, F. K., & Kollet, S. J. (2007). The groundwater-land-surface-atmosphere connection: Soil moisture effects on the atmospheric boundary layer in fully-coupled simulations. *Advances in Water Resources*, 30(12), 2447–2466. https://doi.org/10.1016/j.advwatres.2007.05.018

Maxwell, R. M., Condon, L. E., & Kollet, S. J. (2015). A high-resolution simulation of groundwater and surface water over most of the continental US with the integrated hydrologic model ParFlow v3. *Geoscientific Model Development*, 8(3), 923–937. https://doi.org/10.5194/gmd-8-923-2015

Maxwell, R. M., Lundquist, J. K., Mirocha, J. D., Smith, S. G., Woodward, C. S., & Tompson, A. F. B. (2011). Development of a coupled groundwater atmosphere model. *Monthly Weather Review*, 139, 96–116. https://doi.org/10.1175/2010MWR3392.1

Maxwell, R. M., & Miller, N. L. (2005). Development of a coupled land surface and groundwater model. *Journal of Hydrometeorology*, 6(3), 233–247. https://doi.org/10.1175/jhm422.1

Miguez-Macho, G., & Fan, Y. (2012). The role of groundwater in the Amazon water cycle: 1. Influence on seasonal streamflow, flooding and wetlands. *Journal of Geophysical Research: Atmospheres*, 117(D15). https://doi.org/10.1029/2012jd017539

Miguez-Macho, G., Fan, Y., Weaver, C. P., Walko, R., & Robock, A. (2007). In-corporating water table dynamics in climate modeling: 2. Formulation, validation, and soil moisture simulation. *Journal of Geophysical Research*, 112, 1–16.

Nash, J. E., & Sutcliffe, J. V. (1970). River flow forecasting through conceptual models part I—A discussion of principles. *Journal of Hydrology*, 10(3), 282–290.

Ning, L., Zhan, C., Luo, Y., Wang, Y., & Liu, L. (2019). A review of fully coupled atmosphere-hydrology simulations. *Journal of Geographical Sciences*, 29(3), 465–479. https://doi.org/10.1007/s11442-019-1610-5

Niu, G.-Y., & Yang, Z.-L. (2006). Effects of frozen soil on snowmelt runoff and soil water storage at a continental scale. *Journal of Hydrometeorology*, 7(5), 937–952. https://doi.org/10.1175/jhm538.1

Niu, G.-Y., Yang, Z.-L., Dickinson, R. E., & Gulden, L. E. (2005). A simple TOPMODEL-based runoff parameterization (SIMTOP) for use in global climate models. *Journal of Geophysical Research*, 110(D21). https://doi.org/10.1029/2005jd006111

Niu, G.-Y., Yang, Z.-L., Dickinson, R. E., Gulden, L. E., & Su, H. (2007). Development of a simple groundwater model for use in climate models and evaluation with gravity recovery and climate experiment data. *Journal of Geophysical Research*, 112(D7). https://doi.org/10.1029/2006jd007522

Niu, G.-Y., Yang, Z.-L., Mitchell, K. E., Chen, F., Ek, M. B., Barlage, M., Kumar, A., Manning, K., Niyogi, D., Rosero, E., Tewari, M., & Xia, Y. (2011). The community Noah land surface model with multiparameterization options (Noah-MP): 1. Model description and evaluation with local-scale measurements. *Journal of Geophysical Research*, 116(D12). https://doi.org/10.1029/2010jd015139

Panagos, P., Van Liedekerke, M., Jones, A., & Montanarella, L. (2012). European soil data centre: Response to european policy support and public data requirements. *Land Use Policy*, 29, 329–338. https://doi.org/10.1016/j.landusepol.2011.07.003

Prentice, I. C., Liang, X., Medlyn, B. E., & Wang, Y.-P. (2015). Reliable, robust and realistic: The three Rof next-generation land-surface modelling. *Atmospheric Chemistry and Physics*, 15(10), 5987–6005. https://doi.org/10.5194/acp-15-5987-2015

Rahman, M., Rosolem, R., Kollet, S. J., & Wagener, T. (2019). Towards a computationally efficient free-surface groundwater flow boundary condition for large-scale hydrological modelling. *Advances in Water Resources*, *123*, 225–233. https://doi.org/10.1016/j.advwatres.2018.11.015

Rahman, M., Sulis, M., & Kollet, S. J. (2015). The subsurface–land surface–atmosphere connection under convective conditions. *Advances in Water Resources*, *83*, 240–249. https://doi.org/10.1016/j.advwatres.2015.06.003

Robinson, D. A., Campbell, C. S., Hopmans, J. W., Hornbuckle, B. K., Jones, S. B., Knight, R., Ogden, F., Selker, J., & Wendroth, O. (2008). Soil moisture measurement for ecological and hydrological watershed-scale observatories: A review. *Vadose Zone Journal*, *7*(1), 358–389. https://doi.org/10.2136/vzj2007.0143

Rummler, T., Arnault, J., Gochis, D., & Kunstmann, H. (2018). Role of lateral terrestrial water flow on the regional water cycle in a complex terrain region: Investigation with a fully coupled model system. *Journal of Geophysical Research: Atmospheres*, *124*(2), 507–529. https://doi.org/10.1029/2018jd029004

Senatore, A., Mendicino, G., Gochis, D. J., Yu, W., Yates, D. N., & Kunstmann, H. (2015). Fully coupled atmosphere-hydrology simulations for the Central Mediterranean: Impact of enhanced hydrological parameterization for short and long time scales. *Journal of Advances in Modeling Earth Systems*, *7*, 1693–1715. https://doi.org/10.1002/2015MS000510

Seuffert, G., Gross, P., Simmer, C., & Wood, E. F. (2002). The influence of hydrologic modeling on the predicted local weather: Two-way coupling of a mesoscale weather prediction model and a land surface hydrologic model. *Journal of Hydrometeorology*, *3*(5), 505–523. https://doi.org/10.1175/1525-7541(2002)003<0505:tiohmo>2.0.co;2

Shrestha, P., Sulis, M., Masbou, M., Kollet, S., & Simmer, C. (2014). A scale-consistent terrestrial systems modeling platform based on COSMO, CLM, and ParFlow. *Monthly Weather Review*, *142*, 3466–3483. https://doi.org/10.1175/MWR-D-14-00029.1

Skamarock, W. C., Klemp J. B., Dudhia J., Gill D. O., Liu Z., Berner J., Wang W., Powers J. G., Duda M. G., Barker D. M., & Huang X.-Y. (2019) A Description of the Advanced Research WRF Model Version 4. https://doi.org/10.5065/1DFH-6P97.

Sulis, M., Williams, J. L., Shrestha, P., Diederich, M., Simmer, C., Kollet, S. J., & Maxwell, R. M. (2017). Coupling groundwater, vegetation, and atmospheric processes: A comparison of two integrated models. *Journal of Hydrometeorology*, *18*(5), 1489–1511. https://doi.org/10.1175/jhm-d-16-0159.1

Taylor, C. M. (2015). Detecting soil moisture impacts on convective initiation in Europe. *Geophysical Research Letters*, *42*(11), 4631–4638. https://doi.org/10.1002/2015gl064030

Taylor, C. M., Parker, D. J., & Harris, P. P. (2007). An observational case study of mesoscale atmospheric circulations induced by soil moisture. *Geophysical Research Letters*, *34*(15). https://doi.org/10.1029/2007gl030572

Tijerina, D., Condon, L., FitzGerald, K., Dugger, A., O'Neill, M. M., Sampson, K., Gochis, D., & Maxwell, R. (2021). Continental hydrologic intercomparison project, phase 1: A large-scale hydrologic model comparison over the continental United States. *Water Resources Research*, *57*(7). https://doi.org/10.1029/2020wr028931

Vergnes, J.-P., & Decharme, B. (2012). A simple groundwater scheme in the TRIP river routing model: Global off-line evaluation against GRACE terrestrial water storage estimates and observed river discharges. *Hydrology and Earth System Sciences*, *16*(10), 3889–3908. https://doi.org/10.5194/hess-16-3889-2012

Wagner, S., Fersch, B., Yuan, F., Yu, Z., & Kunstmann, H. (2016). Fully coupled atmospheric-hydrological modeling at regional and long-term scales: Development, application, and a nalysis of WRF-HMS. *Water Resource Research*, *52*, 3187–3211. https://doi.org/10.1002/2015WR018185

Wood, E. F., Roundy, J. K., Troy, T. J., van Beek, L. P. H., Bierkens, M. F. P., Blyth, E., de Roo, A., Döll, P., Ek, M., Famiglietti, J., Gochis, D., van de Giesen, N., Houser, P., Jaffé, P. R., Kollet, S., Lehner, B., Lettenmaier, D. P., Peters-Lidard, C., Sivapalan, M., ... Whitehead, P. (2011). Hyperresolution global land surface modeling: Meeting a grand challenge for monitoring Earthterrestrial water. *Water Resources Research*, *47*(5). https://doi.org/10.1029/2010wr010090

Yang, Z.-L., & Niu, G.-Y. (2003). The versatile integrator of surface and atmosphere processes. *Global and Planetary Change*, *38*(1–2), 175–189. https://doi.org/10.1016/s0921-8181(03)00028-6

Yang, Z.-L., Niu, G.-Y., Mitchell, K. E., Chen, F., Ek, M. B., Barlage, M., Longuevergne, L., Manning, K., Niyogi, D., Tewari, M., & Xia, Y. (2011). The community Noah land surface model with multiparameterization options (Noah-MP): 2. Evaluation over global river basins. *Journal of Geophysical Research*, *116*(D12). https://doi.org/10.1029/2010jd015140

Yeh, P. J.-F., & Eltahir, E. A. B. (2005). Representation of water table dynamics in a land surface scheme. Part I: Model development. *Journal of Climate*, *18*(12), 1861–1880. https://doi.org/10.1175/jcli3330.1

Yin, D., Xue, Z. G., Gochis, D. J., Yu, W., Morales, M., & Rafieeinasab, A. (2020). A process-based, fully distributed soil erosion and sediment transport model for WRF-hydro. *Water*, *12*(6), 1840. https://doi.org/10.3390/w12061840

Yucel, I., Onen, A., Yilmaz, K. K., & Gochis, D. J. (2015). Calibration and evaluation of a flood forecasting system: Utility of numerical weather prediction model, data assimilation and satellite-based rainfall. *Journal of Hydrology*, *523*, 49–66. https://doi.org/10.1016/j.jhydrol.2015.01.042

Zhang, Z., Arnault, J., Wagner, S., Laux, P., & Kunstmann, H. (2019). Impact of lateral terrestrial water flow on land-atmosphere interactions in the Heihe River basin in China: Fully coupled modeling and precipitation recycling analysis. *Journal of Geophysical Research: Atmospheres.*, *124*, 8401–8423. https://doi.org/10.1029/2018jd030174

Zhang, Z., Li, Y., Barlage, M., Chen, F., Miguez-Macho, G., Ireson, A., & Li, Z. (2020). Modeling groundwater responses to climate change in the prairie pothole region. *Hydrology and Earth System Sciences*, *24*(2), 655–672. https://doi.org/10.5194/hess-24-655-2020

Zreda, M., Desilets, D., Ferré, T. P. A., & Scott, R. L. (2008). Measuring soil moisture content non-invasively at intermediate spatial scale using cosmic-ray neutrons. *Geophysical Research Letters*, *35*(21). https://doi.org/10.1029/2008gl035655